ULTRASONIC BEAM PROPAGATION IN CAST STAINLESS STEEL

B. P. Newberry, A. Minachi, and R. B. Thompson

Ames Laboratory
Iowa State University
Ames, IA 50011

INTRODUCTION

The ultrasonic examination of cast stainless steel components found in nuclear reactors has been plagued by problems such as difficulties in achieving sufficient penetration, poor signal-to-noise ratios, false indications, and mislocated flaws. One factor which plays an important role in these problems is anisotropy of the material. Whereas many metal components can be viewed as isotropic, having randomly oriented, equi-axed grains, such is not the case for cast austenitic steels, in which the structure tends to crystallize with the [100]-axis of each grain parallel to the local thermal gradient. A consequence is that the ultrasonic wave speeds vary with direction, which in turn leads to such phenomena as beam skewing and excess beam divergence. The materials, anisotropic or not, can also exhibit large grain sizes which can lead to excess attenuation and background noise. Much effort has been placed on classifying the various microstructures and determining their elastic properties as well as studying beam propagation through them [1-8]. The theoretical modeling of beam propagation in anisotropic and inhomogeneous materials has also received much attention recently [9-16].

The present paper reports on work to develop a theoretical model for ultrasonic beam propagation in anisotropic materials. This is followed by a presentation of experimental data obtained from cast steel specimens of various microstructures, and a comparison with model predictions.

BEAM MODEL

In the previous proceedings the authors [14] presented a Fresnel approximation for Gaussian beam propagation in anisotropic media. The work presented here is an extension of that model to treat arbitrarily shaped beams. The framework for the model, in which one represents a general beam as an angular spectrum of plane waves and makes the Fresnel approximation to the slowness surface, is described in [14] and will not be repeated here.

The previous Gaussian solution represents the lowest order member of a complete set of orthogonal eigenfunction solutions known as the Gauss-Hermite functions. These have been described in detail for isotropic materials [17, 18]. They have now been derived for the anisotropic case and they have been shown to have the form

$$\vec{U}_{mn}(x,y,z) = \vec{d}'(0,0)U_o[w_{x_o}w_{y_o}/w_x(z)w_y(z)]^{1/2}\exp[-j\omega S_o z]$$

$$\exp\{j[(2m+1)\psi_x(z)+(2n+1)\psi_y(z)]\}$$

$$\exp\{-(j\pi/\lambda_z)[(x+Az)^2/q_x(z)+(y+Bz)^2/q_y(z)]\}$$

$$H_m\{[\sqrt{2}/w_x(z)](x+Az)\}H_n\{[\sqrt{2}/w_y(z)](y+Bz)\} \qquad (1)$$

where

$$q_{x,y}(z) = q_{x_o,y_o} + (\Lambda_{x,y}/\lambda_z)z \qquad (2)$$

The various parameters are defined in [14]. The parameters of interest with respect to the anisotropy are the A and B which define the beam skew and the $(\Lambda_{x,y}/\lambda_z)$ which define the curvatures of the slowness surface in the directions transverse to the direction of beam propagation, and hence govern beam divergence.

An arbitrarily shaped beam can now be written as a series of these eigenfunctions

$$\vec{U}(x,y,z) = \sum_{m=0}^{\infty}\sum_{n=0}^{\infty} C_{mn}\vec{U}_{mn}(x,y,z) \qquad (3)$$

where the C_{mn} are complex constant coefficients which are determined by utilizing the orthogonality property of the eigenfunctions along with knowledge of the beam source (i.e., transducer). The coefficients being determined, the displacement field may be computed via Eq. (3).

EXPERIMENTAL BEAM MAPPING

Three cast steel specimens were obtained with fine-grained equi-axed, coarse-grained equi-axed, and columnar grained microstructures, respectively. Through transmitted beam profile maps were obtained in these specimens by a procedure illustrated in Fig. 1. The experiments were performed in an immersion tank with a

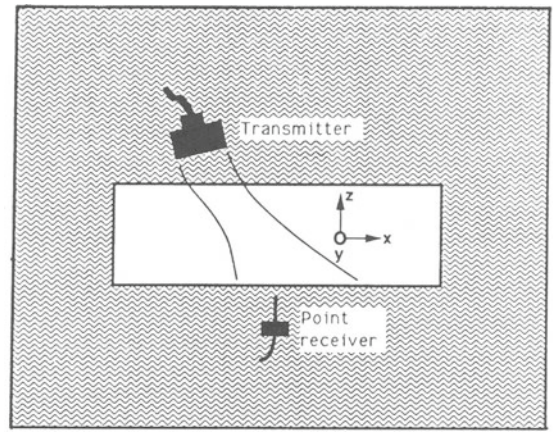

Fig. 1. Schematic of Beam Mapping Experiment.

conventional transducer acting as transmitter and a point receiver (microprobe) used to map the fields emerging from the back surface of the sample. This technique for mapping ultrasonic fields is described in [6, 7].

Figure 2a shows the result of a 2-dimensional mapping of a 45 degree longitudinal wave transmitted through the fine-grained equi-axed sample at 3 MHz. The transmitter was 1″ in diameter and the sample was 5.7 cm thick. The theoretical prediction for this case is shown in Fig. 2b, assuming the material is isotropic with a wavespeed of 0.57 cm/μs. The agreement for this case, as well as for other cases using this sample, is quite good. The material behaves in a very isotropic manner.

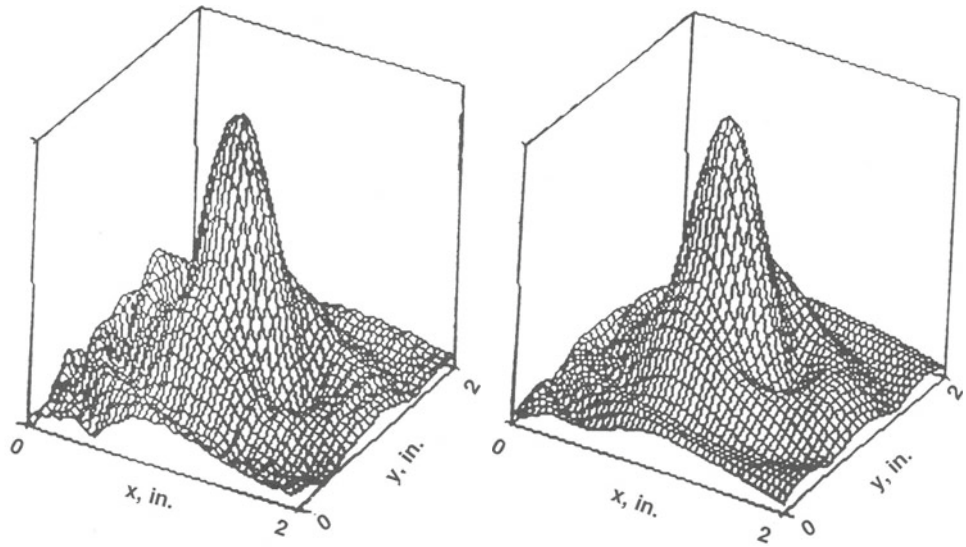

Fig. 2 45 degree L-wave Beam Map through fine-grained equi-axed material: (a) experiment, (b) theory

Figure 3 shows a 1-dimensional beam map (in the x-direction of Fig. 1) of a 45 degree shear wave in the coarse-grained equi-axed sample. This map is at 0.5 MHz as the noise and attenuation in the material was severe at higher frequencies. Again the transmitter is 1″ in diameter and this sample was 5.4 cm thick. The model prediction is shown on the plot also. As can be seen, the model and experiment agree as to an overall beam width. However, the experimental profile has significant amplitude fluctuations across it, presumably due to the large grain structure. The model cannot account for these inhomogeneities.

Wave speed measurements through the sample in various directions suggest that the sample is on average isotropic with wavespeeds of $V_L = 0.58 cm/\mu s$ and $V_T = 0.31 cm/\mu s$.

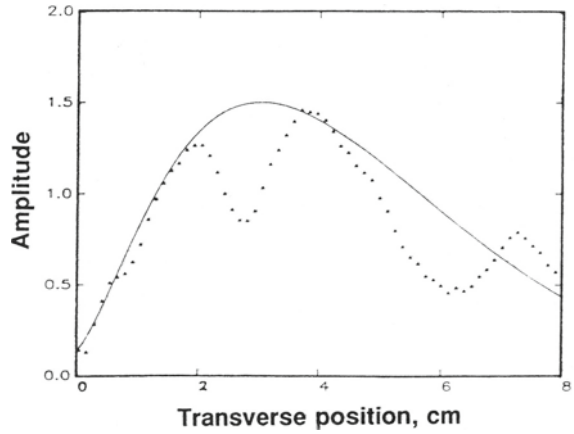

Fig. 3. 45 degree SV-wave Beam profile through coarse-grained equi-axed material. (Solid line-theory, trianges, exp.)

The columnar-grained sample was 6.1 cm thick with the grains aligned in the through thickness direction as shown in Fig. 4. Before modeling beam propagation in this material it was necessary to obtain some information about the elastic constants or, equivalently, the slowness surface. Wave speed measurements in the through thickness direction yielded velocities of $V_L = 0.54 cm/\mu s$ and $V_T = 0.3 cm/\mu s$. These are suggestive of the transverse isotropy commonly assumed for this microstructure, however they are somewhat different than those predicted by a single crystal elastic constant averaging scheme such as that given by Ogilvy [15].

In order to obtain more information, measurements were made of the group velocity angle (θ_g in Fig. 4) as a function of the incident angle in water, θ_i. This is the angle at which the energy actually propagates, which in general will be different from the phase velocity angle θ_p. The difference between the two angles is the beam skew angle. This angle can be measured by scanning the microprobe to find the point on the back surface, relative to the incident point on the front surface, about which the beam is centered. The peak amplitude of the through transmitted beam was also recorded. The results are shown in Figures 5a and 5b for amplitude and θ_g, respectively, for both longitudinal and shear waves.

The L-wave is strongest at about 5 degrees incident angle and it disappears at about 15 degrees incident angle the latter being about what one would expect for the critical angle. The group velocity angle rises sharply at small incident angles and then continues to rise at a slower rate.

The shear wave amplitude rises to a peak at about 18 degrees incident angle and then decreases sharply until about 24 degrees incident angle, after which it becomes stronger again and persists until almost 40 degrees incident angle. This is somewhat puzzling since one would expect the critical angle for shear waves to be about 25 degrees in the water for this material. Also puzzling is the fact that the group velocity angle hovers around zero degrees for the entire range of incident angles. In essence, the shear waves continued to travel straight down through the sample regardless of the incident angle.

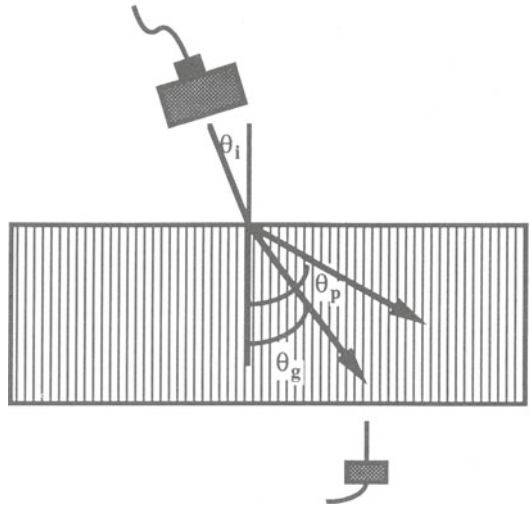

Fig. 4. Schematic of examination of columnar-grained material.

The data in Fig. 5b can be used to estimate the material slowness surface by the following procedure. It can be shown that

$$\frac{dS_z}{dS_x} = -\tan\Theta g \qquad (4)$$

where S_z and S_x are the z and x components of the slowness vector, respectively, and z is the columnar axis. Integrating Eq. (4) yields

$$S_z = \int_0^{S_x} -\tan\theta g \; dS_x + (1/V_o) \qquad (5)$$

where V_o is the velocity along the columnar or through-thickness direction and $S_x = \sin\Theta_i/V_w$, where V_w is the wave speed in water. Equation (5) may be applied to numerically integrate the data of Figure 5b to yield S_z as a function of S_x, which is precisely the slowness surface.

Carrying out this procedure gives the result shown in Fig. 6. The longitudinal slowness surface looks quite like one would expect. The shear surface is reasonable for about half its length and then continues horizontal contrary to expectations (dashed line).

This is related to the earlier observation that the shear wave did not appear to have a normal critical angle. Obviously further work is required to understand this anomaly.

The interesting aspect of this procedure described for determining the slowness surface is that it does not rely on precise velocity measurements other than the one in the normal direction. Also, access is required to only 2 parallel surfaces as opposed to machining coupons to launch waves in various directions. Furthermore, the results of Kriz and Heyliger [19] suggest that the group velocity angle is quite sensitive to the elastic constants and thus might be a good parameter for use in quantifying them.

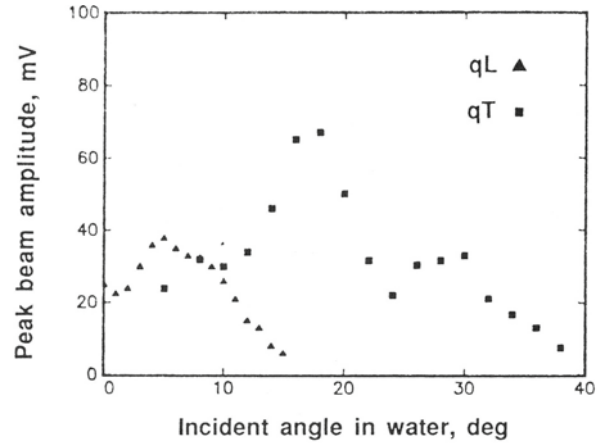

(a)

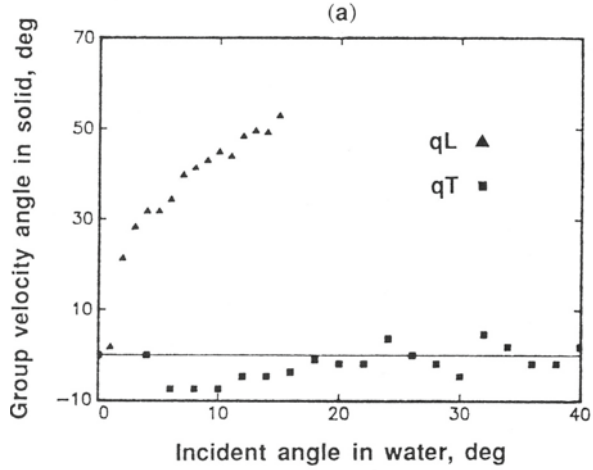

(b)

Fig. 5. (a) Beam amplitude, and (b) group velocity angle, vs. incident angle in water for columnar-grained material.

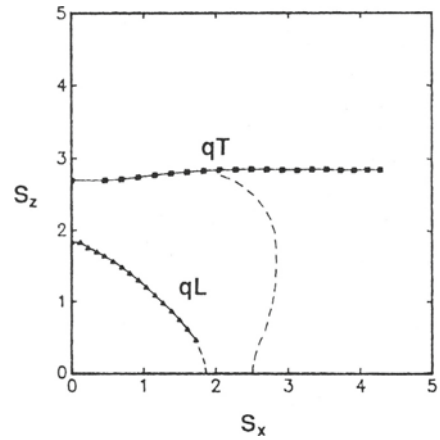

Fig. 6. Slowness curves determined from group velocity angle data, (dashed lines indicate expected behavior of slowness curves).

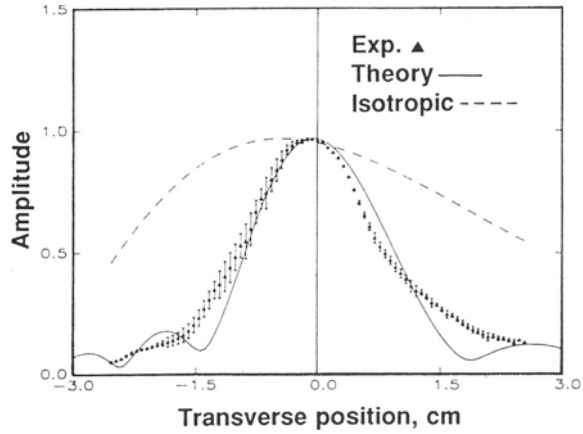

Fig. 7. 45 degree L-wave Beam profile in columnar-grained sample.

The longitudinal slowness curve in Fig. 6 was used to determine the skew and curvature parameters necessary as inputs to the theoretical model. A 1-D experimental map in the x-direction was obtained for a 45 degree L-wave at 2 MHZ using a 0.5″ diameter transducer. The result is shown in Fig. 7 along with the prediction of the anisotropic model as well as the profile predicted if the material were assumed to be isotropic. The anisotropic theory predicts very well the decreased beam spread associated with 45 degree L-waves in transversely isotropic steel.

CONCLUSIONS

The object of this work has been to observe ultrasonic beam behavior in cast stainless steels with various microstructures and to interpret these observations in terms of a model for the beam propagation process which can then hopefully be used to guide future examinations. The model presented herein has shown success for this purpose for isotropic and anisotropic materials. The model will not account at present for the effects of inhomogeneities in the material. The model requires knowledge of the elastic properties associated with the microstructure of a particular material. A technique has been presented to obtain this information in the form of a slowness surface. This worked very well for longitudinal waves in the columnar steel, however the results for shear waves suggest there is still work to be done to fully understand this case.

ACKNOWLEDGMENTS

The authors thank Gerry Posakony and Steve Doctor, both of Battelle-Pacific Northwest Labs, for providing microprobes and the columnar-grained sample, respectively. The remaining samples were obtained from the EPRI NDE Center. This work was sponsored by EPRI under project RP2687-1.

REFERENCES

1. B. R. Dewey, L. Adler, R. T. King, K. V. Cook, Exper. Mechanics 17, 420 (1977).
2. J. Tomlinson, A. Wagg, M. Whittle, in NDE in the Nuclear Industry, R. Natesh, Ed., (American Society of Metals, Metals Park, OH, 1978), p. 64.
3. D. S. Kupperman and K. J. Reimann, ibid, p. 369.
4. L. Adler, K. V. Cook, D. W. Fitting, in Ultrasonic Materials Characterization, H. Berger and M. Linzer, Eds., NBS Special Pub. 596, (NBS, Gaithersburg), p. 533.
5. P. Jeong, Ultrasonic Characterization of Centrifugally Cast Stainless Steel, NP-5246, (EPRI, Palo Alto, CA, 1987).
6. M. S. Good and L. G. Van Fleet, in Review of Progress in QNDE 7, D. O. Thompson, and D. E. Chimenti, Eds., (Plenum, New York, 1988), p. 637.
7. M. S. Good, E. R. Green, S. R. Doctor, in these proceedings.
8. P. Jeong and F. Ammirato, in these proceedings.
9. J. A. Ogilvy, in Review of Progress in QNDE 7, D. O. Thompson, and D. E. Chimenti, Eds., (Plenum, New York, 1988), p. 15.
10. Z. You, R. L. Ludwig, W. Lord, ibid, p. 23.
11. J. L. Rose, A. Pilarski, K. Balasubramanium, J. Dale, D. Diprimeo, ibid, p. 85.
12. A. Norris, ibid, p. 41.
13. R. A. Roberts and D. S. Kupperman, ibid, p. 49.
14. R. B. Thompson and B. P. Newberry, ibid, p. 31.
15. J. A. Ogilvy, Ultrasonics 24, 337 (1986).
16. A. Norris, Wave Motion 9, 1 (1987).
17. R. B. Thompson, T. A. Gray, J. H. Rose, V. G. Kogan, E. F. Lopes, J. Acoust. Soc. Am. 82, 1818, 1987.
18. R. B. Thompson, and E. F. Lopes, in Review of Progress in QNDE 5, D. O. Thompson, and D. E. Chimenti, Eds., (Plenum, New York, 1986), p. 117.
19. R. Kriz and P. Heyliger, in these proceedings.